Biomaterials 35 (2014) 4249–4254

Contents lists available at ScienceDirect

Biomaterials

journal homepage: www.elsevier.com/locate/biomaterials

Responses of *Staphylococcus aureus* bacterial cells to nanocrystalline nickel nanostructures

Zeinab Jahed [a,b], Peter Lin [c], Brandon B. Seo [d], Mohit S. Verma [c], Frank X. Gu [c,**], Ting Y. Tsui [c,d,**], Mohammad R.K. Mofrad [a,b,*]

[a] Molecular Cell Biomechanics Laboratory, Departments of Bioengineering and Mechanical Engineering, University of California Berkeley, 208A Stanley Hall, Berkeley, CA 94720-1762, USA
[b] Physical Biosciences Division, Lawrence Berkeley National Lab, Berkeley, CA 94720, USA
[c] Department of Chemical Engineering, University of Waterloo, 200 University Avenue West, Waterloo, ON N2L 3G1, Canada
[d] Department of Mechanical Engineering, University of Waterloo, 200 University Avenue West, Waterloo, ON N2L 3G1, Canada

ARTICLE INFO

Article history:
Received 18 January 2014
Accepted 31 January 2014
Available online 24 February 2014

Keywords:
Bacteria
Adhesion
Nanostructure
Nanocrystalline
Staphylococcus aureus
Nano-pillar

ABSTRACT

A broad range of human diseases are associated with bacterial infections, often initiated by specific adhesion of a bacterium to the target environment. Despite the significant role of bacterial adhesion in human infectious diseases, details and mechanisms of bacterial adhesion have remained elusive. Herein, we study the physical interactions between *Staphylococcus aureus*, a type of micro-organism relevant to infections associated with medical implants, and nanocrystalline (nc) nickel nanostructures with various columnar features, including solid core, hollow, x-shaped and c-shaped pillars. Scanning electron microscopy results show the tendency of these bacterial cells to attach to the nickel nanostructures. Moreover, unique single bacterium attachment characteristics were observed on nickel nanostructures with dimensions comparable to the size of a single bacterium.

1. Introduction

Staphylococcus aureus (*S. aureus*) is a grape-like shaped bacterium that can adhere to organic [1–3] and metal [1,2,4–10] surfaces. The overall geometry of *S. aureus* is round ("coccus") with diameters approximately ~0.5 μm. This bacterium is a common source of nosocomial infections especially after implant associated surgeries [6,11], such as prosthetic joint implants [12], and heart valves [13]. In addition, they are a common cause of food borne illnesses by adhering to food service surfaces and contaminating food supplies [14].

Moreover, the recent discovery of drug resistance strains of *S. aureus* [15–17], such as methicillin-resistant and oxacillin-resistance *S. aureus*, has led to an emergence of research on bacterial adhesion and survival mechanisms on various surfaces. Several experimental surface coatings and treatment techniques on implant surfaces have been developed [7,9,18–22] with the goal of enhancing osseointegration and reducing bacterial cell adhesion capabilities. Recent studies have suggested a sensitivity of bacteria to nanoscale topographical properties of implant substrates. Wu et al. [23] performed an *in vitro* study on the effects of titanium surface roughness on *Staphylococcus epidermidis* and human osteoblast behavior. These surfaces were prepared with polished, satin, grit-blasted and plasma-sprayed surface finishes. Their results indicated that not only the vertical roughness is important but also the lateral roughness parameters of these small surface features play a role in bacteria attachment. Furthermore, their results showed a preferential colonization of bacteria on micro-rough surfaces, whereas the osteoblasts favored interaction with smooth plasma-sprayed surfaces than with rough satin treated titanium substrates. In a different study, Truong et al. [24] highlighted the effects of nanoscale surface roughness on the adhesion of *S. aureus* and *Pseudomonas aeruginosa* bacteria. Bacteria attachment densities were compared on substrates with different topographical features, but with identical surface chemistry and wettability. Their experiments demonstrated altered bacteria adhesion merely due to surface nano-topography. Specifically, they showed that *S. aureus* tend to attach at significantly higher densities to treated ultrafine-

* Corresponding author. Molecular Cell Biomechanics Laboratory, Departments of Bioengineering and Mechanical Engineering, University of California Berkeley, 208A Stanley Hall #1762, Berkeley, CA 94720-1762, USA. Tel.: +1 510 643 8165; fax: +1 510 642 5835.
** Corresponding authors. Department of Chemical Engineering, University of Waterloo, 200 University Avenue West, Waterloo, ON N2L 3G1, Canada.
E-mail address: mofrad@berkeley.edu (M.R.K. Mofrad).

http://dx.doi.org/10.1016/j.biomaterials.2014.01.080
0142-9612/

grained titanium substrates as compared to untreated bulk substrates. Truong et al. [24] hypothesized that surface nanotopography is a leading factor in controlling bacterial attachment. The effects of nanorough, nanotubular, and nanotextured titanium surfaces on *S. aureus* adhesion were also investigated by Puckett et al. [25]. They demonstrated that bacteria are less likely to adhere to the nanorough Ti surfaces prepared with electron beam evaporation but prefer to attach to nanotubular surfaces.

Despite the industrial and clinical importance of the bacterial surface adhesion, there is no in-depth study on single *S. aureus* cell interactions with well-defined nanometer scale three-dimensional structures. Herein, we present a detailed investigation aimed at understanding how *S. aureus* cells attach to nanocrystalline (nc) nickel columnar nanostructures with various 3D nano-topographical features. These nanostructures include pillars of various cross-sectional geometries, namely solid core, hollow, c-shaped, and x-shaped pillars. These features have outer diameters as small as 220 nm. Three-dimensional mushroom shaped nanostructures were also prepared to understand how these cells interact with overhang topographies. These complex nanostructures were fabricated with electronic beam lithographic techniques and electroplating methods (see Experimental methods). Finally, high-resolution scanning electron microscopy was used to explore the behaviors of individual *S. aureus* cells on these nanometer scale metallic nanostructures of various 3D topographic features comparable with the size of a bacterium.

2. Experimental methods

Nanometer scale nanocrystalline nickel pillars were prepared by using state-of-the-art electronic beam lithographic (EBL) methods and electroplating techniques [26–30]. Fig. 1 illustrates the fabrication steps for these nanostructures. Thin titanium (~20 nm) and gold (~100 nm) films were first deposited on bare silicon substrates using

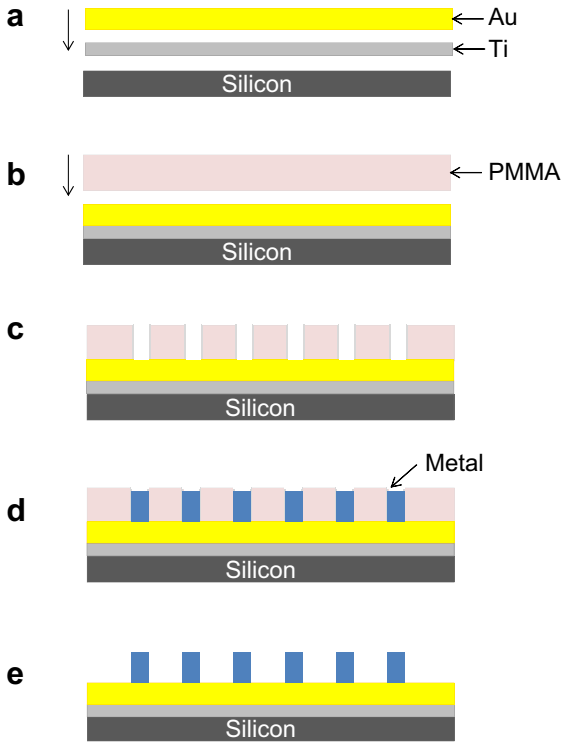

Fig. 1. Nanostructure fabrication process a) electron beam evaporation of 20 nm titanium and 30 nm gold on silicon substrate, b) spin coating of PMMA resist, c) patterning of PMMA resist with ebeam lithography, d) electroplating of desired metal into patterned holes, e) PMMA resist removal via acetone.

electron beam deposition methods. They are then spin coated with Poly (methyl methacrylate) (PMMA) EBL resists. Complex geometric via-hole patterns were produced on these silicon wafers by exposing these thermal plastic films to an electron beam. Nanocrystalline nickel was then deposited in these hole patterns with an electrolyte that contains nickel (II) sulfate hexahydrate (99%, Sigma Aldrich), nickel (II) chloride (98%, Sigma Aldrich), and boric acid (BX0865, EMD Millipore) with concentrations of 300 g/L, 30 g/L, and 30 g/L, respectively. A small amount of saccharine (1.9 g/L) was also added in the plating solution in order to reduce the nickel crystalline size while the current density was maintained at 11.5 ± 2 mA/cm^2 during the plating process. The excess PMMA film was dissolved in acetone after the nickel deposition processes. Detailed transmission electron microscopy analyses revealed a grain size in the range of 9.4 and 13.2 nm for these nickel nanostructures [30].

S. aureus (ATCC 6538) bacteria were generously provided by Dr. Lyndon Jones' laboratory at the University of Waterloo. *S. aureus* bacteria were cultured on trypticase soy agar (TSA) plates by using alginate swabs and incubating the plates at 37 °C overnight. A 2.55% saline solution was prepared and sterilized by using Nalgene filters and ~0.006% of nutrient broth was added to the saline to preserve *S. aureus* during tests. *S. aureus* cells were transferred to saline solution by adding 5 mL of saline to the TSA plate and using alginate swabs to dislodge the bacteria from the plates. *S. aureus* cells were washed with saline solution seven times by centrifugation at 4000 rpm for 10 min. The stock solution of *S. aureus* cells was diluted 10-fold in saline before testing. During a typical test, a drop of diluted *S. aureus* solution was placed on the silicon substrate containing nc-nickel shaped pillars. The specimens were left in the incubator with constant temperatures of ~37 °C. After 6 h, the samples were rinsed with deionized (DI) water to remove cells that are not well adhered to the surfaces and air dried in fume hood for 12 h. Field emission scanning electron beam microscope (Zeiss LEO 1550) was used to inspect how these *S. aureus* cells interact with nickel nanostructures.

3. Results and discussions

Representative 70° tilted scanning electron microscopy (SEM) images of as-fabricated nc-nickel nanostructures with solid core, hollow, c-shaped, and x-shaped pillars are shown in Fig. 2(a–d), respectively. The outer diameter of these vertical pillars is ~1000 nm with a height to diameter aspect ratio of approximately 1.5. Fig. 2(b) shows a representative image of the hollow pillars with average inner diameters of ~840 nm. The c-shaped pillars have an inner diameter of ~760 nm (see Fig. 2(c)). The small openings along the edges of c-shaped pillars allow inspections of the interiors of these nanostructures. Careful SEM inspections of the fabricated pillars with different shapes reveal the pillar exterior sidewalls are extremely smooth and aligned nearly perfectly vertical from the substrate surface. Furthermore, the top surfaces of these nanostructures are flat and slightly rougher than the sidewalls but the roughness still remains in the nanometer scale.

All the nanostructures shown in Fig. 2 were fabricated simultaneously on a single silicon substrate, and are thereby expected to have similar surface chemical compositions and wettability, and differ only in nanometer scale morphology. Furthermore, cell plating was carried out on a single substrate containing all pillar shapes under identical environmental treatments. These nanocrystalline nickel pillars are regularly spaced at a 10 μm center to center distance as shown in Fig. 2(f). In order to better examine how an individual *S. aureus* cell interacts with overhang nano topography, mushroom shaped nc-nickel nanostructures with stem diameters of 220 nm were fabricated as displayed in Fig. 2(e). The micrographs clearly reveal the smooth nickel pillar sidewalls.

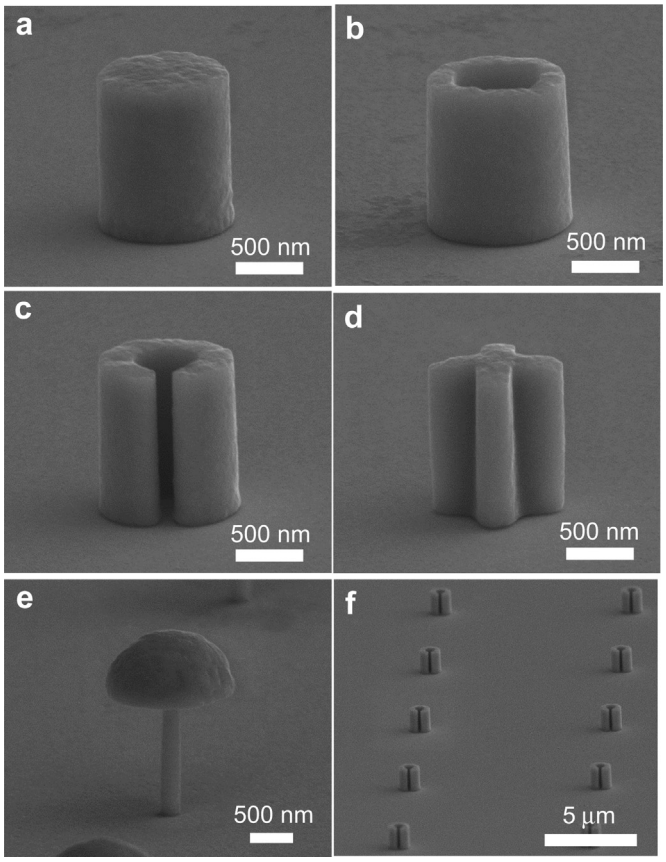

Fig. 2. Representative SEM micrographs revealing pillars with different cross-sectional geometries – (a) solid; (b) hollow (c) c-shaped (d) x-shaped pillars, (e) mushroom shaped nanostructures. An array of c-shaped pillars are shown in (f).

However, the mushroom caps are fairly rough compared to other parts of these nanostructures.

All nanostructures were fabricated in large arrays allowing for the inspection of multiple samples for each cell culture experiment. A representative micrograph revealing a section of the array containing c-shaped pillars is shown in Fig. 2(f). Overall, the dimensions of all fabricated nanostructures were comparable to that of a single *S. aureus* bacterium, allowing for detailed studies on single bacterium responses to the topographical cues of each nanostructure.

Several *S. aureus* cells rested on top of c-shaped pillars, covering the top opening of these pillars as shown in tilted (Fig. 3(a)) and top–down (Fig. 3(b)) SEM micrographs of c-shaped pillars which were exposed to saline solution containing *S. aureus* cells. These microorganisms have diameters of ~500 nm. Other cells adhered to the pillar interface with the substrate below that was coated with a thin layer of gold. As implied by Fig. 3(a), the micro-organism appears to be partially embedded inside the opening but not fallen into the hollow center, likely because it is adhered to the pillar rim. This indicates that this *S. aureus* cell is in fact suspended like a free-standing object with only the edges attached to the nanostructure. In some rare occasions, small bacterial colonies were formed on the top surfaces of a single c-shaped pillar as show in Fig. 3(c) and (d) where two or three cells cluster on the top of the pillar, likely impeding bacteria from entering the opening. This demonstrates that *S. aureus* cells can attach securely with little contact surfaces, such as the top rim of c-shaped pillars. The bacterial adhesion area to the pillar is estimated to be 0.074 μm^2 (see Fig. 3(a) and (b)) Another interesting observation is that a considerable number of *S. aureus* bacteria were able to attach to the vertical, highly curved sidewalls and withstand the DI water rinse process (see Fig. 3(c) and (d)). These results demonstrate a strong adhesion of *S. aureus* on nickel surfaces. Some *S. aureus* cells were also able to enter and fall into the opening instead of residing at the top of the pillars. Fig. 3(e) shows a micrograph of a c-shaped pillar where no bacterium is located at the top opening. However, top–down images revealed that a cell is within the hole and partially adhered to the interior sidewall. In addition, it is possible that no cell is deposited within these holes, such as the pillar shown in Fig. 3(g) and (h). The top–down image clearly shows no *S. aureus* cells are in the pillar center. However, a majority of cells attach and remain on the top of c-shaped pillars rather than within, as shown in the SEM micrograph with the view of 15 pillars in Fig. 3(i). The image clearly shows eleven out of fifteen pillars inspected contain cells attached on the top surface which are indicated with arrows. This demonstrates that c-shaped pillars with proper inner and outer diameters can be an efficient method to capture individual cells.

In addition to the c-shaped pillars, *S. aureus* cells were also deposited on hollow pillars with the same outer diameters of ~1 μm. SEM inspections of these specimens reveal that some of the bacterial cells were successfully attached to the rim of the pillars as shown in Fig. 4. This micrograph shows that the *S. aureus* cell attachment mechanism to the pillars appears to be similar to those observed in the c-shaped pillars shown in Fig. 3(a). In addition to adhesion at the top of the hollow pillars, SEM inspections show cells can penetrate deep into the openings due to the slight larger inner diameter of the hollow pillars when compared to the c-shaped cross-sectional geometries. Cells were located inside the hollow pillar holes as shown in tilted (Fig. 5(a)) and top–down (Fig. 5(b)) SEM micrographs. Cells are clearly not residing at the top of pillar but have penetrated inside the hole (Fig. 5(a)). This penetration was not visible with a 70° tilt view, however, when inspecting the same pillar with a top–down view, a cell can be observed resting at the interior of the hole (Fig. 5(b)) with the cell partially attached to the interior wall of the column. However, it is unclear if the cell is located mid-point or at the bottom of the pillar. Since the cell is constrained within a hollow pillar, it is not certain if it can grow or divide due to the space confinement. As a comparison, the tilted and top-down view of another pillar without a *S. aureus* cell inside the pillar is shown in Fig. 5(c) and (d). The grain microstructure of the gold thin film coated substrate, underneath the hollow pillar, was evident at the bottom of the holes, confirming that the interior of the hollow pillar was empty and no *S. aureus* cells reside within these pillars (Fig. 5(d)).

The affinity of *S. aureus* cell attachment on x-shaped pillars was also studied. SEM micrographs of two pillars with the microorganism attached to the top surface of these complex geometric nanostructures are shown in Fig. 6(a) and (b). These small nickel pillars have wall thicknesses of approximately 300 nm. The images suggest that individual cells are likely to firmly adhere to x-shaped pillars; however, these cells have a lower success rate when compared with c-shaped pillars (see Fig. 3). Out of the eighteen x-shaped pillars inspected, only three demonstrated bacteria adhesion at the top of the pillar (see Fig. 6(c)). One of the possible explanations is that most cells that were initially attached on these nanostructures are detached due to stresses incurred by turbulent flow of DI water during the rinsing process. In contrast, cells that were partially or completely embedded below the surfaces, such as those on the hollow and c-shaped pillars experience smaller turbulent flow stresses during the DI water rinse process.

A few *S. aureus* cells also survived on top of solid core pillars after the DI water rinse as shown in Fig. 7(a) and (b). Depending on the sizes of these cells relative to the pillar diameters, multiple cells may have attached to these pillars (Fig. 7(b)). However, inspections of the eighteen pillars shown in Fig. 7(c) revealed that the probability of

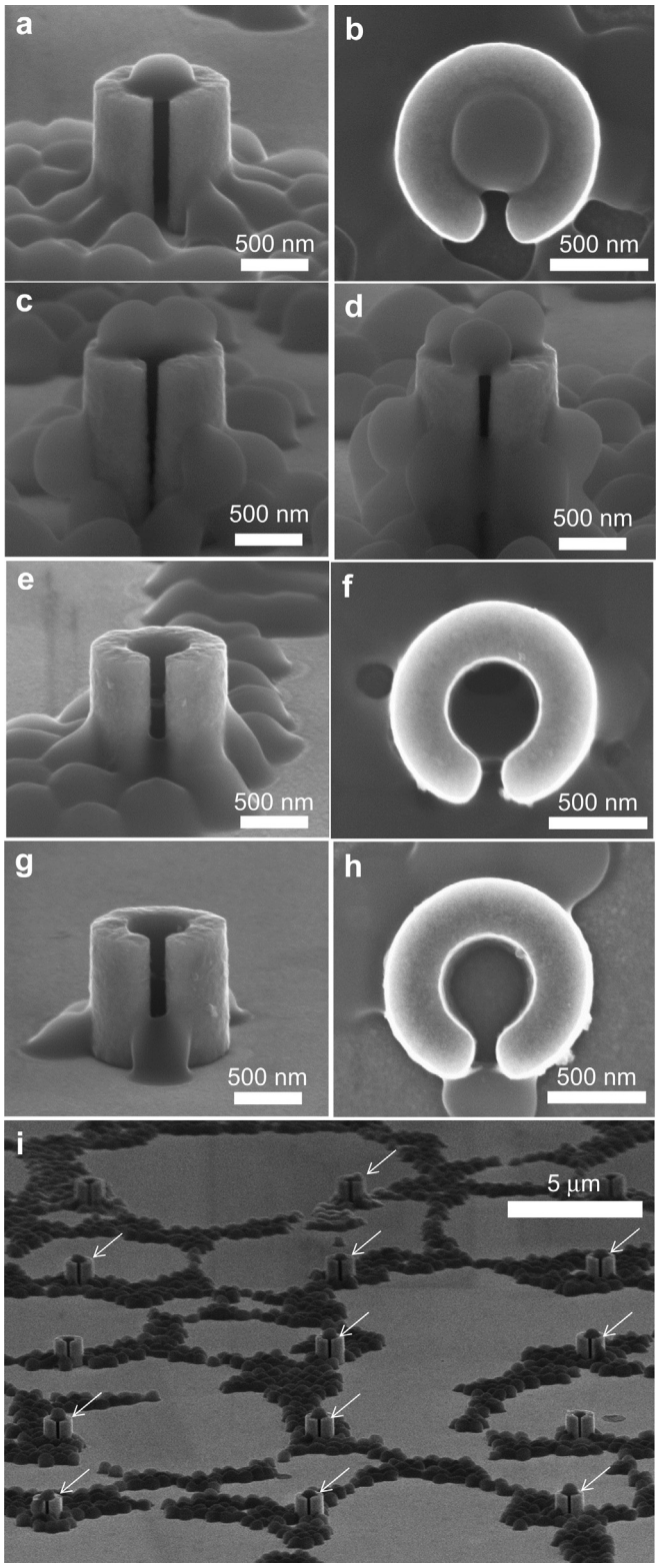

Fig. 3. (a), (b) Tilted and top-down SEM micrographs of the same c-shaped pillar that has been exposed to the *S. aureus* cells, a single *S. aureus* cell is attached to the rim of the c-shaped pillar opening. (c), (d) Tilted SEM micrographs of c-shaped pillars on which small bacteria colonies have formed. (e), (f) Tilted and top–down SEM micrographs of the same c-shaped pillar where an *S. areus* cell has penetrated into the c-shaped hole. (g), (h) Tilted and top-down SEM micrographs of the same c-shaped pillar where no *S. areus* cells has penetrated inside the c-shaped hole. (i). SEM micrographs of c-shaped pillar array with eleven of fifteen covered with *S. auerus* cells at the top surface.

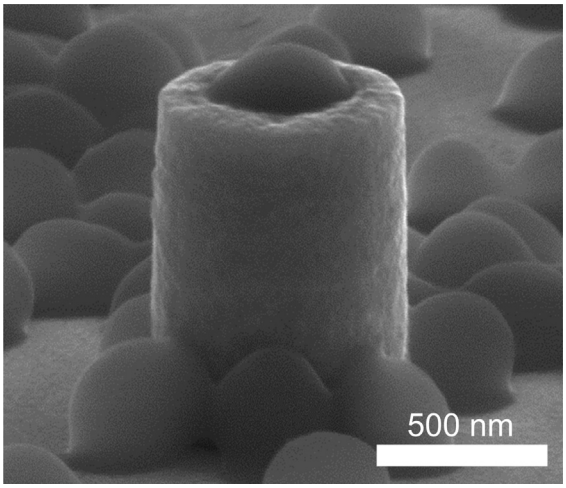

Fig. 4. 70° tilted SEM micrograph revealing a *S. aureus* cell embedded at the top of a hollow pillar.

single microorganisms to successfully attach and survive at the top surface is closer to the x-shaped pillars but significantly lower than the c-shaped pillars. There are only five columns in the figure that show bacterial cells survived on the top of solid core nickel pillars. Finally, for all columnar shapes, the edge interface between the nanostructures and the gold substrate underneath were highly susceptible to bacteria adhesion, and endured the DI rinse. As shown in Figs. 3–7, small colonies of bacteria concentrate at the outer interface between the pillars and the substrate, maximizing surface contact with two contact points, one on the horizontal gold substrate, and another on the pillar sidewall creating strong adhesions.

S. aureus cells were also exposed to nanostructures with overhanging topographic features. Fig. 8(a)–(d) presents typical mushroom-shaped nickel nanostructures that have been exposed to saline solution with bacterial cells. The micrographs (see Fig. 8(b) and (c)) confirmed that the bottom surface of the mushroom cap is very smooth like the stem sidewalls. The mushroom and stem diameters of these nanostructures are ~1400 nm and ~220 nm, respectively. It is interesting to observe that these cells were not only able to attach to the stems of these features but also adhered very well at the base of

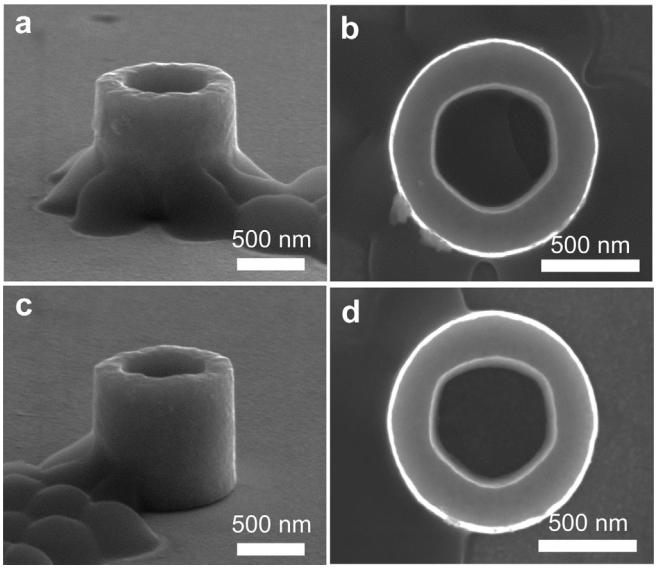

Fig. 5. 70° tilted and top–down SEM micrograph revealing two pillars – one with a cell confined within (a) and (b); and another structure without a cell (c) and (d).

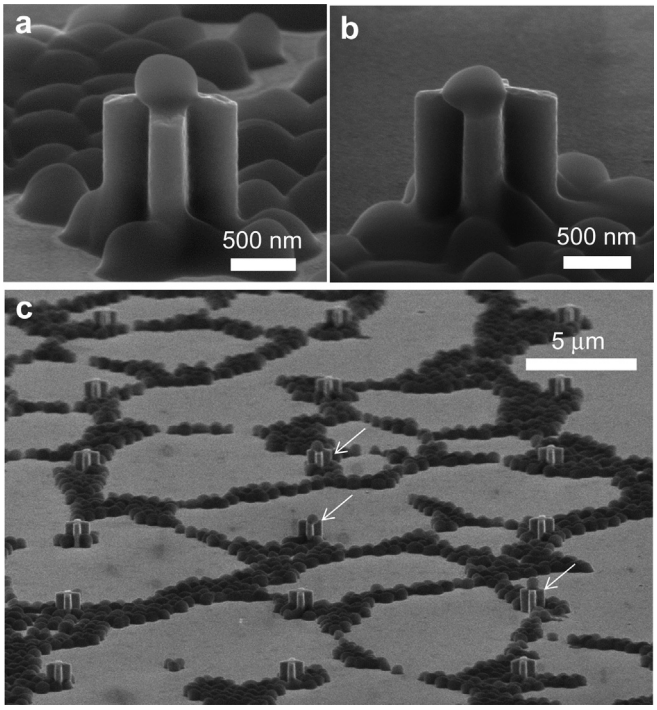

Fig. 6. (a)–(b) 70° tilted SEM micrographs revealing two x-shaped columns with cells adhered on top. (c) Far view of pillar arrays that show only 3 pillars contain cells at their top surfaces.

the mushroom caps or the overhangs. This suggests that the adhesion behaviors of *S. aureus* cells are not constrained by the direction of the gravitational force. Similar to the pillars, the interface between the mushroom caps and the stems, and between the stem and horizontal gold substrate contained a higher density of bacteria. This is

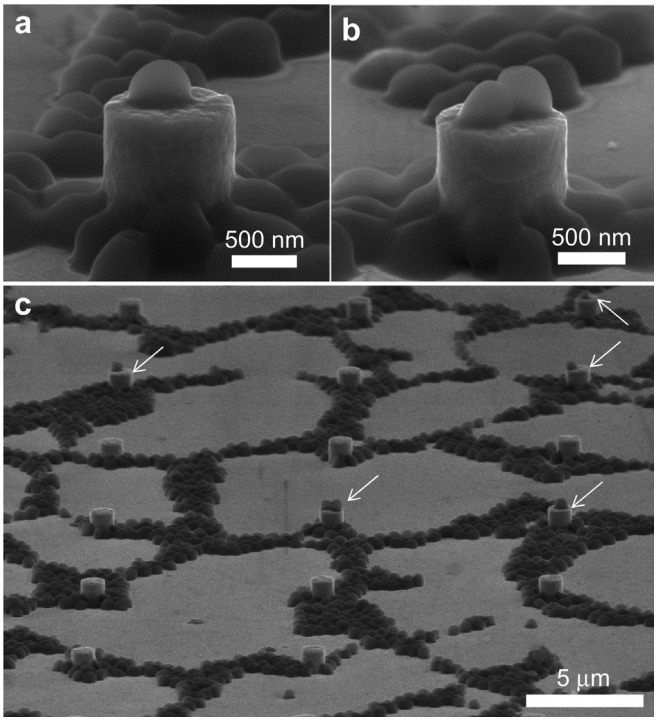

Fig. 7. (a)–(b) 70° tilted SEM micrographs revealing two solid pillars with cells adhered on top. (c) Far view of pillar arrays that show only 5 pillars covered with cells on the top surface.

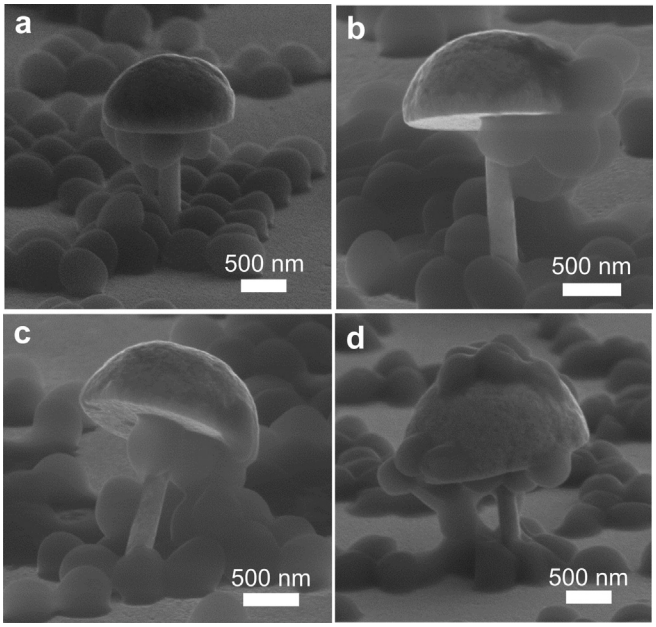

Fig. 8. 70° tilted SEM micrograph revealing four different pillars that has been exposed to *S. aureus* bacterial cells.

conceivably due to the two contact points created at these edges, maximizing bacteria adhesion resulting in stronger adhesions at these locations. Furthermore, *S. aureus* cells adhered to larger mushroom shaped structures with 5 μm diameter stems fabricated on the same substrate, together with ~220 nm mushroom shaped pillars. Significantly more *S. aureus* cells are clustered at the stems of these large structures than the field area (Fig. 9).

Another interesting characteristic observed in Fig. 8(c) and (d) indicates some of the *S. aureus* cells attached to the bottom of the mushroom form links with cells on the horizontal gold substrate through an intermediate chain of cells. Pillars with cells that exhibit

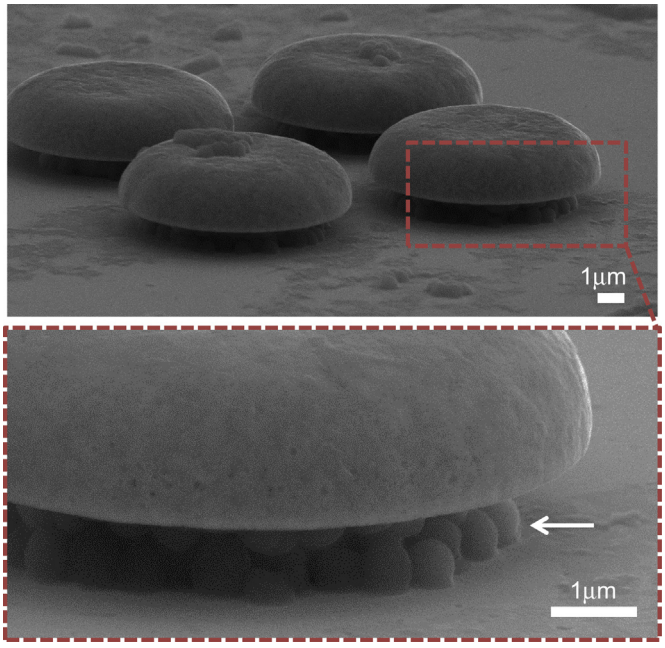

Fig. 9. 70° tilted SEM micrograph revealing mushroom shaped structures with 5 μm diameter stems. Several *S. aureus* cells were clustered at the stem of these structures (arrow).

these behaviors also appear to be bent. However, it is unclear if bending is driven by the shrinkage of the biological components during the drying process. However, the ability for these intermediate cells to maintain the connectivity even after the DI water rinse represents their high adhesion strengths to neighboring bacteria.

Overall, our results demonstrate the sensitivity of bacterial adhesion to nanometer scale topographical features, and mechanical cues of the surface it interacts with. Our observations suggest that bacteria not only maximize their surface area, but also show high resistance to deformation or spreading, hence freestanding on top of hollow cross sections, with a circular adhesion contact area, rather than penetrating inside, or adhering to pillar edges and interfaces forming strong 3D adhesion. One explanation for such behavior is the high protein adsorption on metallic surfaces [31] which allow the adhesion of bacteria to a substrate with no prior modification with extracellular matrix proteins, through ligand/receptor mediated adhesions. A larger contact area will therefore allow a higher number of ligand and receptor to bind per cell, resulting in the formation of a stronger adhesion. Mohamed et al. [32] showed the withstanding of higher shear forces by attached *S. aureus* bacteria as a function of higher receptors expressed per cell.

4. Conclusions

S. aureus cells were successfully deposited on substrates that contain nanocrystalline nickel nanopillars with different cross-sectional geometries and inspected by using high-resolution scanning electron microscopy. The results reveal these cells are able to attach to various small nickel nanostructures and endure DI water rinse but with different survival rates. Nanostructures with via holes that allow cells to embed themselves partially or fully within show a greater probability of success in adhesion to the pillars. In contrast, nickel columns with no holes have the lowest survival rates. Scanning electron micrographs also revealed that *S. aureus* cells are able to attach themselves at the bottom of overhang nanostructures. Finally, using the presented methods, and by varying the geometry, size and spacing of the nanostructures in this study, the effect of nanotopography on *S. aureus* adhesion can further be investigated at the single bacterium level.

Acknowledgments

The authors would like to thank the Natural Sciences and Engineering Council of Canada, NSERC,for their support of this research project through Discovery and RTI grants as well as Graduate Fellowships to ZJ and MSV. In addition, financial support through National Science Foundation via the CAREER award (CBET-0955291) to MRKM is gratefully acknowledged. The authors gratefully acknowledge critical support and infrastructure provided for this work by the Emerging Communications Technology Institute at the University of Toronto. ZJ would like to thank the Department of Chemical Engineering, and the Nanomechanics Research Institute at the University of Waterloo for supporting her as a visiting scholar.

References

[1] Gristina AG, Hobgood CD, Webb LX, Myrvik QN. Adhesive colonization of biomaterials and antibiotic resistance. Biomaterials 1987;8:423–6.
[2] Oga M, Sugioka Y, Hobgood CD, Gristina a G, Myrvik QN. Surgical biomaterials and differential colonization by *Staphylococcus epidermidis*. Biomaterials 1988;9:285–9.
[3] Francois P, Schrenzel J, Stoerman-Chopard C, Favre H, Herrmann M, Foster TJ, et al. Identification of plasma proteins adsorbed on hemodialysis tubing that promote *Staphylococcus aureus* adhesion. J Lab Clin Med 2000;135:32–42.
[4] Barth E, Myrvik Q, Wagnert W, Gristina AG. In vitro and in vivo comparative colonization of *Staphylococcus aureus* and *Staphylococcus epidermidis* on orthopaedic orthopaedic implant materials. Biomaterials 1989;10:325–8.
[5] Cordero J, Munuera L, Folgueira MD. Influence of metal implants on infection. An experimental study in rabbits. J Bone Jt Surg Br 1994;76.
[6] Melcher GA, Claudi B, Schlegel U, Perren SM, Printzen G, Munzinger J. Influence of type of medullary nail on the development of local infection. J Bone Jt Surg 1994;76.
[7] Arenas M a, Pérez-Jorge C, Conde A, Matykina E, Hernández-López JM, Pérez-Tanoira R, et al. Doped TiO_2 anodic layers of enhanced antibacterial properties. Colloids Surf B Biointerfaces 2013;105:106–12.
[8] Harris LG, Meredith DO, Eschbach L, Richards RG. *Staphylococcus aureus* adhesion to standard micro-rough and electropolished implant materials. J Mater Sci Mater Med 2007;18:1151–6.
[9] Wang X, Wang G, Liang J, Cheng J, Ma W, Zhao Y. *Staphylococcus aureus* adhesion to different implant surface coatings: an in vitro study. Surf Coatings Technol 2009;203:3454–8.
[10] Teterycz D, Ferry T, Lew D, Stern R, Assal M, Hoffmeyer P, et al. Outcome of orthopedic implant infections due to different staphylococci. Int J Infect Dis 2010;14:e913–8.
[11] Harris LG, Foster SJ, Richards RG. An introduction to *Staphylococcus aureus*, and techniques for identifying and quantifying *S. aureus* adhesins in relation to adhesion to biomaterials: review. Eur Cell Mater 2002;4:39–60.
[12] Moran E, Byren I, Atkins BL. The diagnosis and management of prosthetic joint infections. J Antimicrob Chemother 2010;65(Suppl. 3):iii45–54.
[13] Renzulli A, Della Corte A, Torella M, Dialetto G, Cotrufo M. Mitral and aortic valve endocarditis due to *Staphylococcus lugdunensis*. Tex Hear Inst J; 2000:67–9.
[14] Da Silva Meira QG, de Medeiros Barbosa I, Alves Aguiar Athayde AJ, de Siqueira-Júnior JP, de Souza EL. Influence of temperature and surface kind on biofilm formation by Staphylococcus aureus from food-contact surfaces and sensitivity to sanitizers. Food Control 2012;25:469–75.
[15] Karska-Wysocki B, Bazo M, Smoragiewicz W. Antibacterial activity of *Lactobacillus acidophilus* and *Lactobacillus casei* against methicillin-resistant *Staphylococcus aureus* (MRSA). Microbiol Res 2010;165:674–86.
[16] Chiu H-C, Lee S-L, Kapuriya N, Wang D, Chen Y-R, Yu S-L, et al. Development of novel antibacterial agents against methicillin-resistant *Staphylococcus aureus*. Bioorg Med Chem 2012;20:4653–60.
[17] Williamson JC, Virata SR, Raasch RH, Kylstra J a. Oxacillin-resistant *Staphylococcus aureus* endophthalmitis after ganciclovir intraocular implant. Am J Ophthalmol 2000;129:554–5.
[18] Campoccia D, Baldassarri L, Pirini V, Ravaioli S, Montanaro L, Arciola CR. Molecular epidemiology of *Staphylococcus aureus* from implant orthopaedic infections: ribotypes, agr polymorphism, leukocidal toxins and antibiotic resistance. Biomaterials 2008;29:4108–16.
[19] Huo K, Zhang X, Wang H, Zhao L, Liu X, Chu PK. Osteogenic activity and antibacterial effects on titanium surfaces modified with Zn-incorporated nanotube arrays. Biomaterials 2013;34:3467–78.
[20] Rochford ET, Poulsson AH, Salavarrieta Varela J, Lezuo P, Richards RG, Moriarty TF. Bacterial adhesion to orthopaedic implant materials and a novel oxygen plasma modified PEEK surface. Colloids Surf B Biointerfaces 2013;113C:213–22.
[21] Hu X, Neoh K-G, Shi Z, Kang E-T, Poh C, Wang W. An in vitro assessment of titanium functionalized with polysaccharides conjugated with vascular endothelial growth factor for enhanced osseointegration and inhibition of bacterial adhesion. Biomaterials 2010;31:8854–63.
[22] Papa R, Artini M, Cellini A, Tilotta M, Galano E, Pucci P, et al. A new anti-infective strategy to reduce the spreading of antibiotic resistance by the action on adhesion-mediated virulence factors in Staphylococcus aureus. Microb Pathog 2013;63:44–53.
[23] Wu Y, Zitelli JP, TenHuisen KS, Yu X, Libera MR. Differential response of Staphylococci and osteoblasts to varying titanium surface roughness. Biomaterials 2011;32:951–60.
[24] Truong VK, Lapovok R, Estrin YS, Rundell S, Wang JY, Fluke CJ, et al. The influence of nano-scale surface roughness on bacterial adhesion to ultrafine-grained titanium. Biomaterials 2010;31:3674–83.
[25] Puckett SD, Taylor E, Raimondo T, Webster TJ. The relationship between the nanostructure of titanium surfaces and bacterial attachment. Biomaterials 2010;31:706–13.
[26] Burek MJ, Greer JR. Fabrication and microstructure control of nanoscale mechanical testing specimens via electron beam lithography and electroplating. Nano Lett 2010;10:69–76.
[27] Jahed Z, Evans RD, Burek MJ, Tsui TY. Mechanical properties of columnar submicron cobalt structures with various cross-sectional geometries. Scr Mater 2012;67:463–6.
[28] Jin S, Xie S, Burek MJ, Jahed Z, Tsui TY. Microstructure and mechanical properties of sub-micron zinc structures. J Mater Res 2012;27:2140–7.
[29] Jin S, Burek MJ, Evans RD, Jahed Z, Leung MC, Evans ND, et al. Fabrication, microstructure, and mechanical properties of high strength cobalt sub-micron structures. Mater Sci Eng A 2012;552:104–11.
[30] Seo BB, Jahed Z, Burek MJ, Tsui TY. Influence of grain size on the strength size dependence exhibited by sub-micron scale nickel structures with complex cross-sectional geometries. Mater Sci Eng A 2013;596:275–84.
[31] Nakanishi K, Sakiyama T, Imamura K. On the adsorption of proteins on solid surfaces, a common but very complicated phenomenon. J Biosci Bioeng 2001;91:233–44.
[32] Mohamed N, Rainier TR, Ross JM. Novel experimental study of receptor-mediated bacterial adhesion under the influence of fluid shear. Biotechnol Bioeng 2000;68:628–36.